Available online at www.sciencedirect.com
ScienceDirect
Journal of the European Ceramic Society 27 (2007) 979–985
www.elsevier.com/locate/jeurceramsoc

# Field assisted sintering of electro-conductive $ZrO_2$-based composites

K. Vanmeensel, A. Laptev, O. Van der Biest, J. Vleugels *

*Department of Metallurgy and Materials Engineering (MTM), K.U. Leuven, Kasteelpark Arenberg 44, Heverlee B-3001, Belgium*

Available online 9 June 2006

**Abstract**

In order to reveal the fundamentals of the field assisted sintering technique (FAST), also known as spark plasma sintering (SPS), the evolution of the current density and temperature distribution in the punch-die-sample set-up during FAST of $ZrO_2$–TiN powder mixtures was modeled by finite element calculations supported by in situ measured electrical and thermal input data. The thermal and electrical properties of partially sintered composite powder compacts were estimated using theoretical mixture rules, allowing to calculate the current density and temperature distribution inside the tool and the specimen during the FAST sintering process. The electrical properties of the sintering composite powder compact, and hence the thermal distribution in the sinter set-up, changed drastically during densification once percolation occurred. Based on the calculated thermal distribution inside the composite powder compact, an optimal tool-powder compact design was determined in order to process electrically conductive $ZrO_2$–TiN composites from electrical insulating powder compacts within minutes with high reproducibility.


*Keywords:* Spark Plasma Sintering (SPS); Electrical properties; Thermal properties; $ZrO_2$; Composites

## 1. Introduction

The field assisted sintering technique (FAST), also known as spark plasma sintering (SPS) or pulsed electric current sintering (PECS), belongs to a class of sintering techniques that employ a pulsed DC current to intensify sintering.[1] Some general advantages of field assisted sintering, compared to traditional hot pressing or hot isostatic pressing, are technological advantages such as short processing time, the use of high heating rates hereby minimizing grain growth often leading to improved mechanical,[2] physical[3] or optical[4] properties and elimination of the need of sintering aids.

Lately, a lot of research is focused on a more fundamental understanding of the sintering process. Recent studies focused on the effect of (a) the electrical current and (b) the DC pulse pattern on the solid state reactivity of Mo and Si,[5,6] on the effect of contact resistances on the temperature distribution during the FAST process in case of monolithic fully densified materials[7,8] and on the enhanced sintering kinetics and diffusion mechanisms during the sintering process.[9]

Furthermore, high heating rates, especially in combination with short dwell times, can cause temperature gradients and subsequently sintering inhomogeneity leading to non-uniform microstructural and mechanical properties of the sintered parts.[10–12] Therefore, the temperature field within the sintering powder compact during FAST sintering should be understood and controlled as well as possible. Up till now, most researchers controlled the temperature during a FAST sintering cycle by focusing a pyrometer on the outer die wall surface, leading to an underestimation of the sintering temperature. In order to correlate this temperature with the temperature of the sintering powder compact inside the die, the temperature distributions within the whole tool-specimen system should be known. The most practical way to find this out is theoretical modelling.

Previous research performed at our institute pointed out the importance of both the contact resistances induced by the graphite papers and of the electrical properties of the specimen. When a fully dense TiN compact was placed inside the FAST equipment, the radial temperature gradient at high temperatures (>1500 °C) was much higher compared to the gradient in a fully dense 3Y–$ZrO_2$ compact.[8] Based on these observations, the thermal cycle controlling pyrometer was positioned more strategically i.e. focussing on the bottom of a borehole inside the upper punch of a graphite tool set-up (Fig. 1). In this way, the temperature at the specimen's centre differed less than 5 °C from the temperature measured by the central pyrometer, independent on the sample's electrical properties. Furthermore, it

* Corresponding author. Tel.: +32 16 32 12 64; fax: +32 16 32 19 92.
*E-mail address:* jozef.vleugels@mtm.kuleuven.be (J. Vleugels).

0955-2219/$ – see front matter © 2006 Elsevier Ltd. All rights reserved.
doi:10.1016/j.jeurceramsoc.2006.04.142

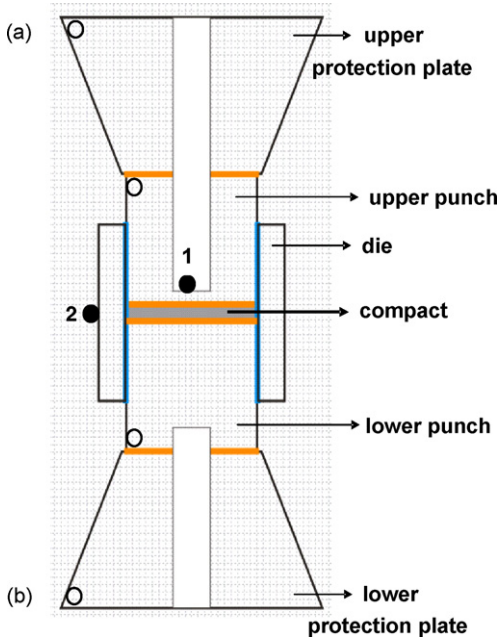


Fig. 1. Cross-section of the tool used during FAST cycles. The position of the 1 mm diameter boreholes (O ) used for voltage measurements or for the positioning of thermocouples: (a) upper protection plate; (b) lower protection plate. The vertical and four horizontal graphite papers are highlighted. Points 1 and 2 are the focus points of the two pyrometers used. The white areas indicate the position of the boreholes.

was suggested that the radial temperature gradient in electrically conductive samples can be reduced by reducing the radiation heat losses from the outer die wall surface. Therefore, the die can be surrounded by porous carbon felt insulation.

In the present work, the developed finite element method and ANSYS code were used to predict the thermal gradients inside a sintering $ZrO_2$–TiN (60/40) composite during the FAST process. The simulated data were in very good agreement with the experimentally measured temperature and resistance values. Interrupted sintering cycles were performed in order to correlate the shrinkage of the powder compact with its changing thermal and electrical properties.

## 2. Experimental procedures

$ZrO_2$–TiN (60/40) powder compacts were prepared by ball milling 3Y–$ZrO_2$ (Daiichi HSY-3U, $d_{50} = 20$ nm), TiN (H.C. Starck, grade C, $d_{50} = 1.4$ μm) and a small amount (0.75 wt.% with respect to the Y–$ZrO_2$ content) of $Al_2O_3$ (Taimicron, TM-DAR, $d_{50} = 100$ nm) in a multidirectional Turbula T2C mixer.

Experiments were performed on a FCT FAST device (Type HP D 25/1, FCT Systeme, Rauenstein, Germany). More details about the used FAST device can be found elsewhere.[8] During the presented experiments, a pulse-pause combination of 10–5 ms is used throughout all the experiments. Controlling the power, which is done by controlling the voltage difference over the electrodes, generates a preset time–temperature profile. In this way, the current flowing through the specimen-punch-die set-up is controlled. During the experiments, the temperature is measured by a central pyrometer with a focus point at the bottom

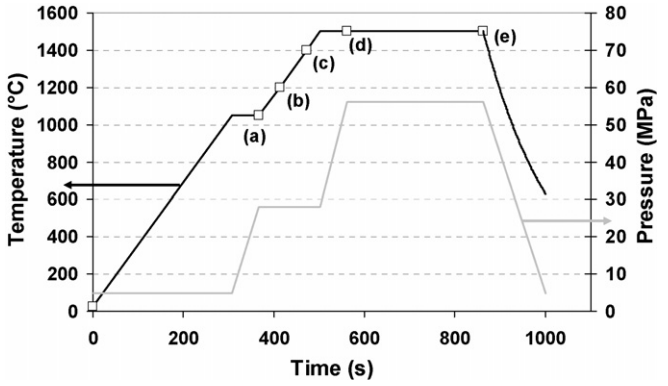


Fig. 2. Pressure–temperature profile used during processing of the $ZrO_2$–TiN (60/40) composites. In case interrupted sintering cycles were performed, the current was switched off at the points indicated by the open symbols. In any case, the total processing time, including cooling, was less than 25 min.

of the central borehole of the graphite set-up, 2.88 mm from the bottom of the upper punch and 5.125 mm from the centre of a 4.25 mm thick sample inside the die (Fig. 1). The temperature of the die is measured by a second two-colour pyrometer, focussed on the outer die wall surface at the same height as the centre of the compact (Fig. 1).

A standard temperature and pressure cycle is shown in Fig. 2 and consists of six segments: (1) applying a constant current until the central pyrometer reached a temperature of 450 °C, the onset temperature of the pyrometer, (2) applying a linearly increasing current resulting in a heating rate of 200 °C/min in the temperature region between 450 and 1050 °C, (3) applying a constant current during the dwell period at 1050 °C (during this dwell period the pressure was increased from 5 to 28 MPa), (4) applying a linearly increasing current resulting in a heating rate of 200 °C/min in the temperature region between 1050 and 1500 °C, (5) applying a constant current during the dwell period at 1500 °C (during the first minute of this dwell period with a total length of 6 min, the pressure is increased from 28 to 56 MPa, and (6) applying no current during cooling from 1500 °C down to room temperature and lowering the pressure at the same time. The interrupted sintering cycles were performed at different temperature and pressure combinations as indicated by the open symbols in Fig. 2.

The electrical resistivities of fully dense, hot pressed $ZrO_2$–TiN composites with a TiN content varying between 35 and 95 vol.% TiN were measured at room temperature using a four point contact technique.

## 3. Results and discussion

### 3.1. Interrupted sintering cycles using a $ZrO_2$–TiN (60/40) powder compact

Typical microstructures of FAST sintered $ZrO_2$–TiN (60/40) composite powder compacts obtained at 1050 °C (a), 1200 °C (b), 1400 °C (c), 1500 °C for 1 min (d) and 1500 °C for 6 min (e) are shown in Fig. 3. Table 1 describes the evolution of the density of the sintering compacts as a function of temperature and applied pressure. The major part of the densification takes place

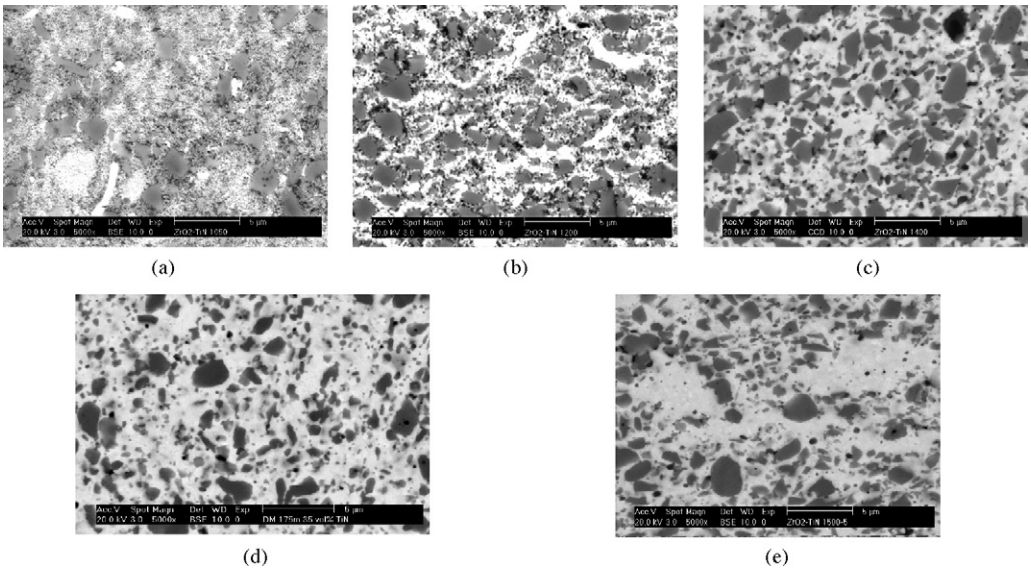


Fig. 3. Representative microstructures of the partially sintered powder compacts obtained at different interrupted stages of sintering, as indicated in Fig. 2: (a) 1050 °C to 28 MPa, (b) 1200 °C at 28 MPa, (c) 1400 °C at 28 MPa, (d) 1500 °C at 56 MPa for 1 min and (e) 1500 °C at 56 MPa for 6 min. White: $ZrO_2$; grey: TiN; black: $Al_2O_3$.

Table 1
Evolution of the density (% TD) of the $ZrO_2$–TiN (60/40) powder compact as a function of sintering temperature and pressure

| Temperature (°C) | Pressure (MPa) | % TD |
|---|---|---|
| 1050 | 28 | 56 |
| 1200 | 28 | 75 |
| 1400 | 28 | 94 |
| 1500 for 1 min | 56 | 97 |
| 1500 for 6 min | 56 | 100 |

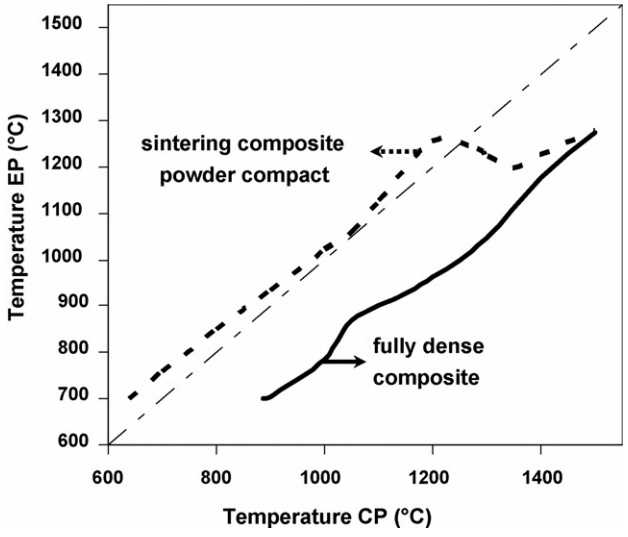


Fig. 4. Plot of the temperature profile recorded by the external pyrometer (EP) vs. the temperature profile recorded by the central pyrometer (CP) for a $ZrO_2$–TiN (60/40) powder compact (thick dotted line) and a fully dense $ZrO_2$–TiN (60/40) compact (thick full line). The thin dotted line represents an equal temperature reading for the external and central pyrometer.

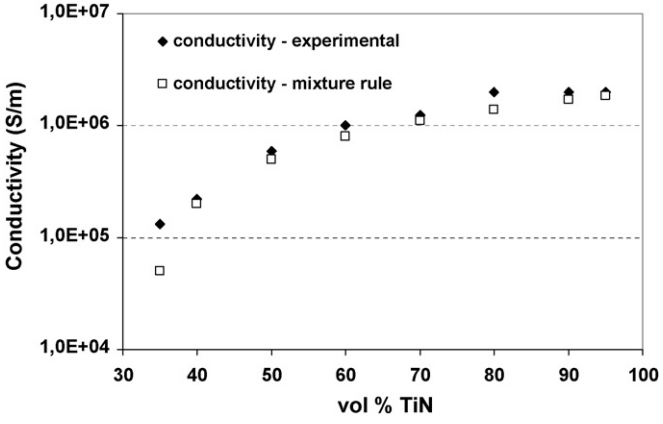


Fig. 5. Comparison between the experimentally measured electrical conductivity and the electrical conductivity calculated by the Polder–Van Santen mixture rule for fully dense hot pressed $ZrO_2$–TiN composites with a varying TiN content between 35 and 95 vol.%. All measurements were performed at room temperature.

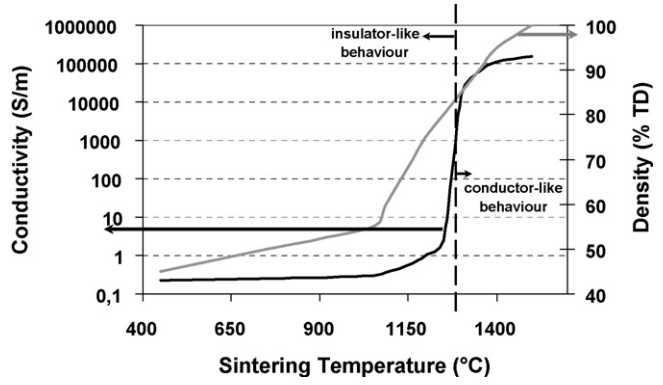


Fig. 6. The evolution of the calculated electrical conductivity and the measured relative density of a sintering $ZrO_2$–TiN (60/40) powder compact, plotted as function of the sintering temperature.

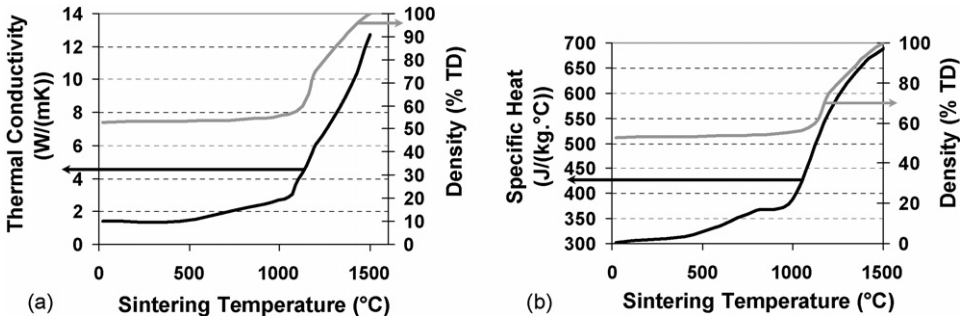


Fig. 7. Calculated thermal conductivity (a) and specific heat (b) of a sintering $ZrO_2$–TiN (60/40) composite powder compact.

between 1050 and 1400 °C. From 1200 °C on (Fig. 3(b)), the TiN particles start to form an interconnected particle network. At that moment, the residual porosity in the sample is about 25% (Table 1), while the remaining 75% of the compact volume consists of the $ZrO_2$ matrix (44.5%), the secondary TiN phase (29.7%) and the $Al_2O_3$ sinter additive (0.8%). During the final dwell time at 1500 °C, the remaining porosity, predominantly located close to the TiN grain boundaries (Fig. 3(e)), disappears and grain growth of the $ZrO_2$ matrix grains occurs.

Additionally, two sintering experiments, both following the complete sintering cycle as described in the previous section, were performed. During the first experiment, a $ZrO_2$–TiN (60/40) powder compact was placed inside the graphite die, while a fully dense $ZrO_2$–TiN (60/40) composite was used during the second experiment. During both experiments, the temperature at the bottom of the borehole inside the upper punch as well as at the die wall surface at the same height as the centre of the compact was recorded. Fig. 4 shows the temperature profile recorded by the pyrometer focusing on the die versus the temperature profile recorded by the central pyrometer. In case of the sintering powder compact, the die temperature equals the temperature on the bottom of the borehole in the upper punch up to about 1250 °C, while in case of a fully dense sample the die temperature is always much lower than the temperature recorded by

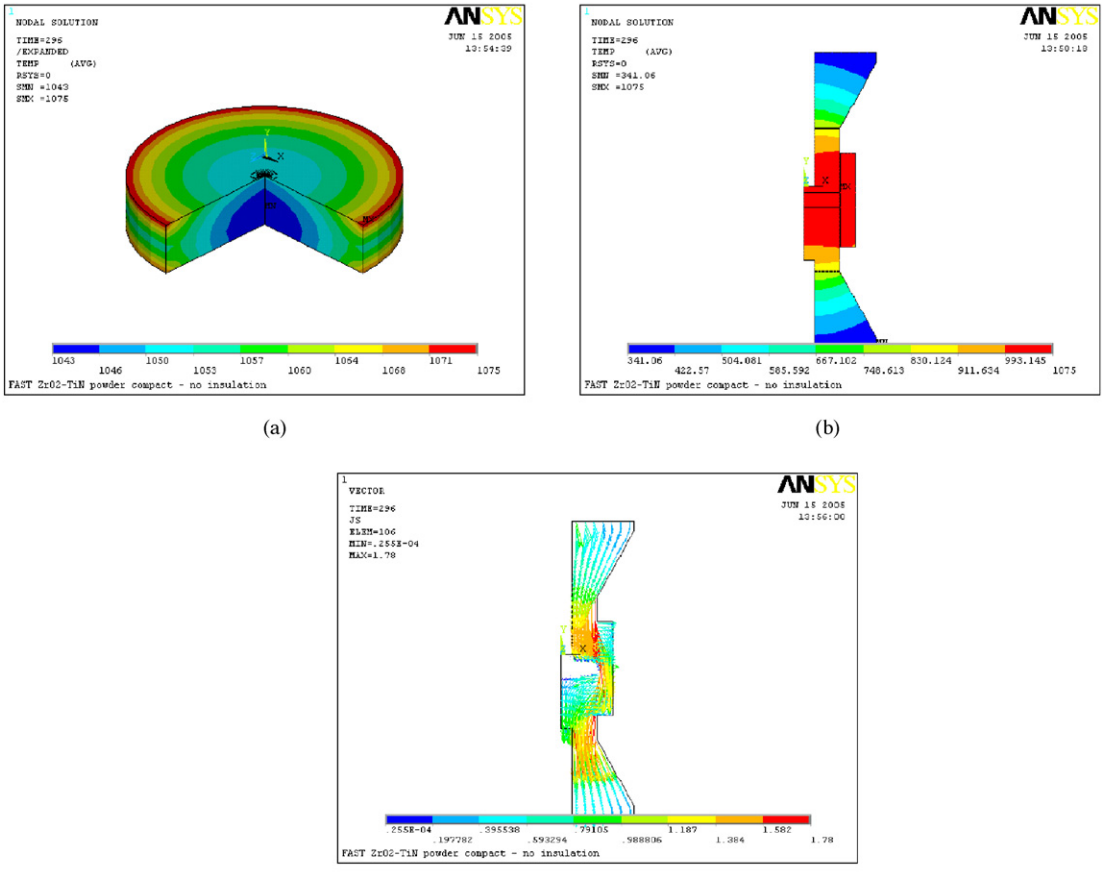


Fig. 8. Temperature distribution inside a sintering $ZrO_2$–TiN (60/40) composite powder compact (a), inside the tool (b) and the concomitant current densities in the tool at a temperature of 1050 °C (after applying a pressure of 28 MPa).

the central pyrometer. In case of the sintering powder compact, the die temperature starts to differ significantly from the temperature recorded by the central pyrometer at 1300 °C. During the final dwell at 1500 °C, the temperature difference between the two pyrometers is the same, independent on whether a powder compact or a fully dense compact was placed inside the die. The temperature difference between both pyrometers was estimated to be 220 °C, which is similar to the temperature difference between the central pyrometer and the die in case a fully dense TiN compact is placed inside the die.[8]

### *3.2. Application and validation of the rule of mixtures to determine the thermal and electrical properties of the sintering $ZrO_2$–TiN (60/40) composite powder compact*

The electrical conductivity as a function of temperature of a fully dense $ZrO_2$–TiN (60/40) compact was estimated using literature values for the electrical conductivity of pure 3 mol% $Y_2O_3$ stabilised $ZrO_2$[13,14] and pure TiN[15–16] in combination with the Polder–Van Santen mixture rule[17] assuming (a) a homogeneous dispersion of the TiN particles in the $ZrO_2$ matrix and (b) a spherical TiN powder shape. The validity of this approximation was tested by comparing calculated conductivities of $ZrO_2$–TiN composites with a varying TiN content between 35 and 95 vol.% with experimentally determined conductivities of hot pressed $ZrO_2$–TiN composites. Fig. 5 confirms the excellent agreement between the calculated and the measured data.

In order to estimate the influence of densification on the changing electrical properties of a sintering $ZrO_2$–TiN (60/40) powder compact, porosity was introduced into the Polder–Van Santen mixture rule as a third, electrically insulating component. The evolution of the calculated electrical conductivity and the measured relative density of the sintering $ZrO_2$–TiN (60/40) powder compact are plotted as a function of temperature in Fig. 6. A sudden increase in electrical conductivity is observed between 1250 and 1300 °C. Therefore, it is assumed that the electrical behaviour of a sintering $ZrO_2$–TiN (60/40) composite powder compact changes from 'insulator-like' at temperatures below 1200 °C to 'conductor-like' at temperatures above 1300 °C. Within this 100 °C temperature range, an electrically conductive powder particle network is formed within the sintering compact.

Besides the drastic change in electrical properties, the thermal properties of the sintering powder compact change as well. The thermal conductivity of the sintering powder compact was estimated using a mixture rule originally proposed by Argento and Bouvard.[18] The specific heat of the sintering compact was estimated from the specific heat of the fully dense compact by multiplication with its theoretical density. Both the calculated thermal conductivity and calculated specific heat of the sinter-

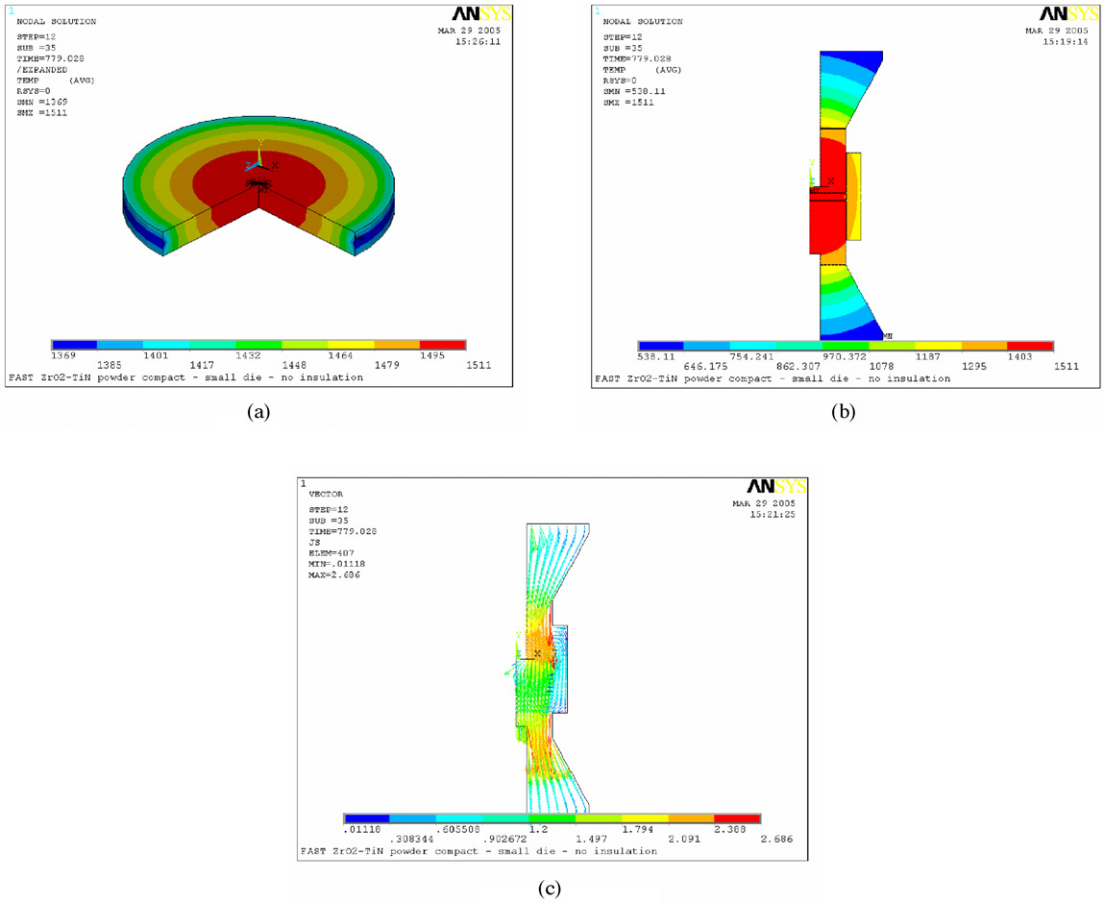


Fig. 9. Temperature distribution inside a sintering $ZrO_2$–TiN (60/40) composite powder compact (a), inside the tool (b) and the concomitant current densities in the tool at a temperature of 1500 °C (after applying a pressure of 56 MPa).

ing $ZrO_2$–TiN (60/40) composite powder compact are shown in Fig. 7.

### 3.3. Simulation of the current and temperature distribution during FAST sintering of a $ZrO_2$–TiN (60/40) composite powder compact

The calculated properties of the sintering $ZrO_2$–TiN (60/40) composite powder compact were inserted in a self-developed FE code to simulate the thermal and electrical distributions inside the tool and the sample during FAST processing.[8] The sample height of the loose powder compact was about 8.5 mm, while a 4.25 mm thick fully dense composite sample is obtained after sintering. The temperature distributions at 1050 °C, as recorded by the central pyrometer, inside the composite powder specimen and the graphite tool are shown in Fig. 8(a) and (b), while the current density in the tool is presented in Fig. 8(c). It is worth noticing that at this temperature, the current density in the die is much higher compared to the current density in the specimen, resulting in a relatively small thermal gradient in the sample of about 30 °C with a slight overheating of the sample edge compared to the sample centre. At the final sintering temperature, the radial temperature gradient in the specimen is much larger (140 °C). During this stage, the hottest zone is located in the sample centre (Fig. 9(a)). Since the sintering composite powder compact becomes electrically conductive during the sintering cycle, the current path is changed from upper punch ⇒ die ⇒ lower punch at low temperatures (Fig. 8(c)) towards upper punch ⇒ compact ⇒ lower punch at high temperatures (Fig. 9(c)). Since the amount of current flowing through the die is limited during the final sintering stage, the die is mainly heated through conduction from the punches and the compact. Moreover, a reasonable amount of heat is lost by radiation from the graphite die wall at high temperatures. Both these factors, the limited current flowing through the die and the radiation heat losses, induce a large temperature difference between the die and the centre of the compact during the final sintering stage (Fig. 9(b)). This radial temperature gradient is also observed in the sample (Fig. 9(c)).

In order to check the validity of the finite element model, the recorded temperature difference between the die and the central pyrometer was compared with the simulated values (Fig. 10).

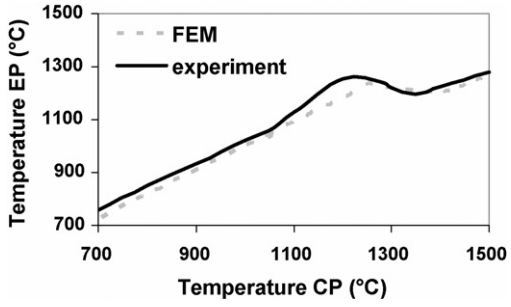


Fig. 10. Comparison between the experimentally determined and simulated temperature difference between the central pyrometer (CP) and the external pyrometer (EP) in case a $ZrO_2$–TiN (60/40) composite powder compact is placed inside the die.

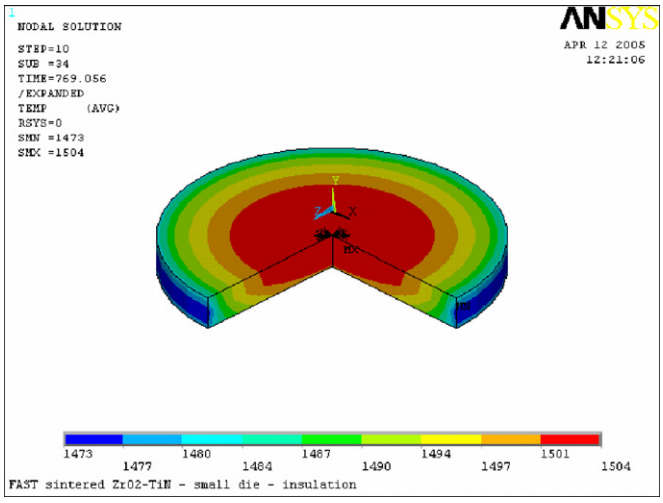


Fig. 11. Radial temperature distribution inside a $ZrO_2$–TiN (60/40) composite powder compact during the final stage of sintering (1500 °C at 56 MPa) in case the graphite die was surrounded with porous carbon felt insulation.

Fig. 10 confirms the excellent agreement between experimentally measured temperatures and the temperatures predicted using the finite element code. In the same way, the radial temperature gradient inside the $ZrO_2$–TiN (60/40) sample was predicted to be about 140 °C during the final stage of sintering. In order to obtain a more homogeneous temperature field and concomitantly sintering behaviour, a porous carbon felt insulation, minimising the radiation heat losses from the outer die wall surface, was placed around the die. The simulated temperature distributions, shown in Fig. 11, point out the effectiveness of this measure, since the radial temperature gradient was reduced from 140 °C (Fig. 9(a)) to 31 °C (Fig. 11).

## 4. Conclusions

When $ZrO_2$ based, electrically conductive, ceramic composites are to be processed using the field assisted sintering technique, one should take into account the changing electrical and thermal properties of the sintering powder compact. Once a percolating path is formed inside the sintering powder compact, the temperature and current profile change very quickly leading to a large radial temperature gradient inside the specimen during the final stage of the sintering process.

In this work, the changing thermal and electrical properties of a sintering $ZrO_2$–TiN (60/40) composite powder compact were determined performing interrupted FAST sintering cycles in combination with literature based mixture rules. Following these calculations, percolation should occur once the powder compact contains 33% electrically conductive TiN phase, corresponding to a theoretical density of 83% of a $ZrO_2$–TiN powder compact containing 40 vol.% of TiN. The interrupted sintering experiments indicate that this density is obtained between 1200 and 1300 °C, which is confirmed by a drastic increase in the temperature difference between a central pyrometer, focusing on the bottom of a borehole in the upper punch, and an external pyrometer, focusing on the die wall surface, in this temperature region. Since the electrical behaviour of the sintering composite powder

compact changes from 'insulator-like' to 'conductor-like' when percolation occurs, the current density in the die is suddenly decreased. This sudden drop of the current flow through the die in combination with the radiation heat losses from the graphite die surface, induce a radial temperature gradient in the tool and the sintering compact. Surrounding the die with porous graphite felt insulation proved to minimise the radiation heat losses and decreased the radial temperature gradient inside the sintering compact from about 140 to 30 °C.

## Acknowledgements

This work is financially supported by the GROWTH program of the Commission of the European Communities under project contract No. G5RD-CT2002-00732. Prof. Laptev thanks the K.U. Leuven Research Council for his 8-month research fellowship (No. F/02/096).

## References

1. Groza, J. R., *Field Assisted Sintering, ASM Handbook*, *Vol 7, Powder Metal Technologies and Applications, ed. ASM International. Handbook Committee*, Ohio (USA), 1998, pp. 583–589.
2. Shen, Z., Zhao, Z., Peng, H. and Nygren, M., Formation of tough interlocking microstructures in silicon nitride ceramics by dynamic ripening. *Nature*, 2002, **417**, 266–269.
3. Khor, K. A., Cheng, K. H., Yu, L. G. and Boey, F., Thermal conductivity and dielectric constant of spark plasma sintered aluminium nitride. *Mater. Sci. Eng. A*, 2003, **347**, 300–305.
4. Su, X., Wang, P., Chen, W., Shen, Z., Nygren, M., Yibing, C. and Yan, D., Effects of composition and thermal treatment on infrared transmission of Dy-α-sialon. *J. Eur. Ceram. Soc.*, 2004, **24**, 2869–2877.
5. Anselmi-Tamburini, U., Garay, J. E. and Munir, Z. A., Fundamental investigations on the spark plasma sintering/synthesis process III. Current effect on reactivity. *Mater. Sci. Eng. A*, 2005, **407**, 24–30.
6. Anselmi-Tamburini, U., Garay, J. E., Groza, J. R. and Munir, Z. A., Fundamental investigations on the spark plasma sintering/synthesis process I. Effect of dc pulsing on reactivity. *Mater. Sci. Eng. A*, 2005, **394**, 132–138.
7. Zavaliangos, A., Zhang, J., Krammer, M. and Groza, J. R., Temperature evolution during field activated sintering. *Mater. Sci. Eng. A*, 2004, **379**, 218–228.
8. Vanmeensel, K., Laptev, A., Hennicke, J., Vleugels, J. and Van der Biest, O., Modeling of the temperature distribution during field assisted sintering. *Acta Mater.*, 2005, **53**, 4379–4388.
9. Shen, Z. and Nygren, M., Microstructural prototyping of ceramics by kinetic engineering: applications of spark plasma sintering. *Chem. Rec.*, 2005, **5**, 173–184.
10. Jayaseelan, D. D., Ueno, S., Ohji, T. and Kanzaki, S., Differential sintering by improper selection of sintering parameters during pulse electric current sintering. *J. Am. Ceram. Soc.*, 2004, **87**(1), 159–161.
11. Srivatsan, T. S., Ravi, B. G., Petraroli, M. and Sudarshan, T. S., The microhardness and microstructural characteristics of bulk molybdenum samples obtained by consolidating nanopowders by plasma pressure compaction. *Int. J. Refrac. Met. Hard Mater.*, 2002, **20**, 181–186.
12. Wang, S. W., Chen, L. D. and Hirai, T., Microstructure inhomogeneity in $Al_2O_3$ sintered bodies formed during the plasma-activated sintering process. *J. Mater. Sci. Lett.*, 1999, **18**, 1119–1121.
13. Lee, Y.-K. and Park, J.-W., Microstructure and electrical conductivity of yttria-stabilized zirconia electrolyte thin plates produced by the doctor blade method. *J. Mater. Sci. Lett.*, 1997, **16**, 678–682.
14. Gödickemeier, M., Miochel, B., Orliukas, A., Bohac, P., Sasaki, K., Gauckler, L., Heinrich, H., Schwander, P., Kostorz, G., Hoffmann, H. and Frei, O., Effect of intergranular glass films on the electrical conductivity of 3Y–TZP. *J. Mater. Res.*, 1994, **9**(5), 1228–1240.
15. Pierson, H. O., *Handbook of Refractory Carbides and Nitrides – Properties, Characteristics, Processing and Applications*. Noyes Publications, 1996, pp. 183–188 [Chapter 11: Interstitial Nitrides: Properties and General Characteristics].
16. Weimer, A. W., *Carbide, Nitride and Boride Materials Synthesis and Processing*. Chapman & Hall, 1997, pp. 653–654 [Appendix D].
17. Bánhegyi, G., Comparison of electrical mixture rules for composite. *Colloid Polym. Sci.*, 1986, **264**, 1030–1050.
18. Argento, C. and Bouvard, D., Modeling the effective thermal conductivity of random packing of spheres through densification. *Int. J. Heat Mass Transfer*, 1996, **39**(7), 1343–1350.